*Mineralogical Magazine, February 2005, Vol. 69(1), pp. 1–20*

# Computational investigation of Al/Si and Al/Mg ordering in aluminous tremolite amphiboles

E. J. PALIN[1,2,*,†], M. T. DOVE[1], M. D. WELCH[1,2] AND S. A. T. REDFERN[1]

[1] Department of Earth Sciences, University of Cambridge, Downing Street, Cambridge CB2 3EQ, UK
[2] Department of Mineralogy, Natural History Museum, Cromwell Road, London SW7 5BD, UK

**ABSTRACT**

The $^{[4]}$Al/Si and $^{[6]}$Al/Mg order-disorder behaviour of minerals in the tremolite-tschermakite solid solution (namely, end-member tschermakite and the 50:50 composition, magnesiohornblende) has been investigated by Monte Carlo simulation, using a model Hamiltonian in which atomic interaction parameters $J_i$ were derived from empirical lattice energy calculations, and chemical potential terms $\mu_j$ (to express the preferences of cations for particular crystallographic sites) were derived from *ab initio* methods. The simulations performed were increasingly complex. Firstly, ordering in one tetrahedral double chain with Al:Si = 1:3 (tschermakite) was simulated. Although the low-temperature cation distribution in this system was ordered, there was no phase transition (due to the quasi-one-dimensional nature of the system). Next, interactions between tetrahedral Al:Si = 1:3 double chains were included, and a phase transition was observed, with the cation distribution in one double chain lining up with respect to that in the next. Finally, interactions between tetrahedral and octahedral sites were incorporated, to model the whole unit cell, and compositions corresponding to tschermakite and magnesiohornblende were investigated. The whole-cell simulation results compare favourably with experimental conclusions for magnesiohornblende, in that Al at *T*1 is preferred over Al at *T*2, and Al at *M*2 is favoured over that at *M*1 and *M*3, but the significant amount of Al at *M*1 is at odds with experimental observation.

**KEYWORDS:** cation ordering, tremolite–tschermakite, magnesiohornblende, amphibole, computer simulation.

## Introduction

IN this paper we present a computer simulation study of the order-disorder behaviour of two compositions in the aluminous tremolite (tremolite–tschermakite) solid solution: the fictive end-member, tschermakite, $^{[A]}\square\,^{[8]}Ca_2{}^{[6]}(Mg_3Al_2)^{[4]}[Si_6Al_2]O_{22}(OH)_2$ and the 50:50 composition, magnesiohornblende, $^{[A]}\square\,^{[8]}Ca_2{}^{[6]}(Mg_4Al)^{[4]}[Si_7Al]O_{22}(OH)_2$. This work follows on from our previous simulation studies of cation ordering in minerals, in which we have investigated the effects of both the number of ordering species and the number of types of crystallographic sites across which these species may order. Our work on Al/Si ordering in muscovite (Palin *et al.*, 2001) investigated the behaviour of two types of cations on one type of site. Our study of phengite (Palin *et al.*, 2003*a*) explored the ordering behaviour of three types of cation across two types of site, namely tetrahedral Al/Si and octahedral Al/Mg ordering, and the nature of the coupling between these ordering processes. Subsequently, we investigated the behaviour of three ordering species across one type of site, in the case of Al/Fe/Mg ordering in the general dioctahedral phyllosilicate sheet (Sainz-Diaz *et al.*, 2003*a*,*b*; Palin *et al.*, 2004). Finally, in our work on glaucophane (Palin *et al.*, 2003*b*), we investigated Al/Mg ordering across three crystallographically distinct sites.

* E-mail: ejp24@cam.ac.uk
DOI: 10.1180/0026461056910232
† Present address: Davy-Faraday Research Laboratory, the Royal Institution of Great Britain, 21 Albemarle Street, London W1S 4BS, UK

© *2005 The Mineralogical Society*

Though we have previously studied coupled ordering processes (phengite) and ordering across several site types (glaucophane), we have not previously studied both phenomena in one mineral system. The present study addresses this; we explore two ordering processes and a total of five crystallographically distinct sites taking part in ordering in aluminous tremolites.

The interest in the order-disorder behaviour of tremolite–tschermakite minerals stems from their potential importance in geothermobarometry. If a better understanding could be gained of the thermodynamics governing cation ordering in this system, amphiboles may offer an opportunity to create geothermometers in conditions where other minerals are not appropriate. For example, studies of divalent cation ordering in olivines (Redfern *et al.*, 1997), which have been suggested as potential geothermometers, show that $Mg/Mn^{2+}$ and $Mg/Fe^{2+}$ exchange can be sufficiently fast that high-*T* cation distributions are not preserved in natural samples, with the result that geothermometers based on olivine may be inaccurate. By contrast, it appears (Raudsepp *et al.*, 1987) that exchange of heterovalent cations is much slower, meaning that crystallization temperatures could be deduced from, e.g. Mg/Al distributions. Clearly, aluminous tremolites, with $^{[6]}$Al/Mg and $^{[4]}$Al/Si, could be appropriate for such an application. This study is not intended to provide conclusive results with respect to geothermobarometry, but the computational approach that we have used yields simulated Mg/Al site occupancies and cation distributions, which may be of use in further investigations.

A further motivation for study is that the tschermakite end-member is not known to exist in nature – tschermakitic bulk compositions yield

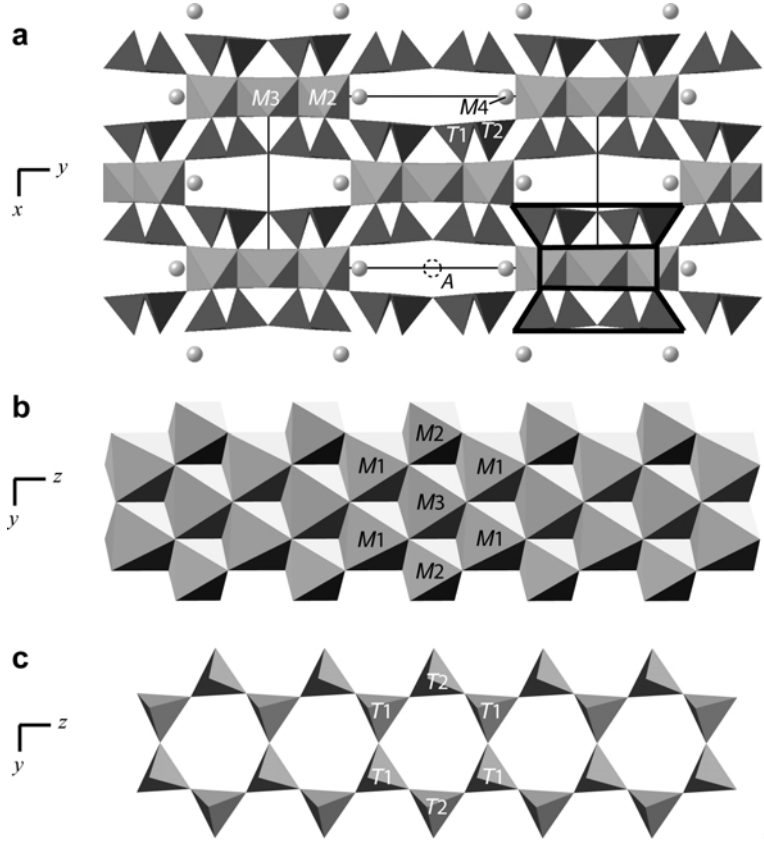


FIG. 1. (*a*) The amphibole structure viewed down *z*. The *M*4 (six- to eight-fold), tetrahedral and octahedral sites are labelled (*M*1 is obscured by the *M*2 and *M*3 sites in this projection), and the *A* site is shown as vacant (dotted circle) here. The box indicates the unit cell, and also shown at the bottom right (in cartoon form) is one 'I-beam' unit. (*b*) The octahedral ribbon showing *M*1–3 sites. (c) The tetrahedral double chain showing *T*1 and *T*2 sites.

Al-rich amphibole and other phases such as chlorite, spinel and forsterite (Jenkins, 1994). However, tschermakite remains interesting with reference to comparative studies across the solid solution. Moreover, solid solutions at the tremolite-rich end of the series do occur naturally, and also can be synthesized; the most tschermakite-rich composition that can be synthesized along the tremolite-tschermakite join is usually considered to be magnesiohornblende. A computational study of this system could provide a new perspective on the reasons for the compositional limits of stability in this series.

### *Structure of tremolite–tschermakite amphiboles*

The amphibole structure is shown in Fig. 1. The sites which are relevant in this study are the two distinct tetrahedral (*T*) sites, *T*1 and *T*2, and the three distinct octahedral (*M*) sites, *M*1, *M*2 and *M*3 (we also use *O* here to signify octahedral sites). The tetrahedral sites are corner-linked to form a tetrahedral double chain (so named by analogy with the single-chain structure of pyroxenes), with *T*1 sites occurring along the centres of the double chains and *T*2 sites along the edges, giving a *T*1:*T*2 ratio of 1:1, and eight *T* sites per formula unit. The octahedral sites are edge-linked to form ribbons, with *M*3 sites running down the centre, *M*2 sites along the edges and *M*1 sites between the two, such that the ratio of numbers of *M* sites is *M*1:*M*2:*M*3 = 2:2:1, and there are five *M* sites per formula unit. One octahedral ribbon is sandwiched between two tetrahedral ribbons, to produce the familiar 'I-beam' structural unit. The other sites shown in the diagram are the distorted, highly coordinated *M*4 site (important in defining the major amphibole groups – calcic, sodic-calcic, alkali) and the *A* site, situated between adjacent I beams.

Tremolite and tschermakite end-member components are related by the Tschermak substitution $^{[6]}Mg^{[4]}Si \rightleftharpoons {}^{[6]}Al^{[4]}Al$, and so we must consider Al both on the octahedral and the tetrahedral sites, and the possibility of coupling between octahedral and tetrahedral ordering schemes. Many experimental studies have been undertaken in order to determine the ordering behaviour of Al in aluminous tremolites (e.g. Hawthorne *et al.*, 2000; Jenkins *et al.*, 1997), and on other closely-related minerals such as pargasite and pargasitic hornblendes (e.g. Raudsepp *et al.*, 1987; Welch *et al.*, 1994). Pargasite, $^{[A]}Na^{[8]}Ca_2{}^{[6]}(Mg_4Al)^{[4]}[Si_6Al_2]O_{22}(OH)_2$, is relevant to this study as it has the same octahedral cation ratio as magnesiohornblende, and the same tetrahedral cation ratio as tschermakite.

To date, the following deductions have been made for ordering across octahedral sites. Hawthorne (1981, 1983) argued from bond-valence considerations that in these minerals $^{[6]}Al$ should occur at *M*2. Raudsepp *et al.* (1987) concluded from IR, MAS-NMR and structure refinement studies that $^{[6]}Al$ should occur at *M*2 and *M*1/*M*3, a finding which was later supported by MAS-NMR and IR investigations by Welch *et al.* (1994). Later studies by X-ray structure refinement (Oberti *et al.*, 1995*a*), neutron diffraction (Welch and Knight, 1999), IR spectroscopy (Della Ventura *et al.*, 1999), IR and triple-quantum NMR (Hawthorne *et al.*, 2000) revised this to *M*2 and *M*3, but not *M*1. For the tetrahedral cation behaviour, bond-valence calculations (Hawthorne, 1981, 1983, 1997) suggest that Al should order preferentially at *T*1. This proposition was corroborated by $^{29}Si$ MAS NMR studies (Welch *et al.*, 1998). It was also concluded by Oberti *et al.* (1995*b*) that an Al content of more than two tetrahedral Al atoms per formula unit leads to Al at *T*2, but that less Al-rich compositions had Al at *T*1. Additionally, a recent computational/experimental study (Najorka and Gottschalk, 2003) of both tetrahedral and octahedral order in tremolite-tschermakite assumed that $^{[4]}Al$ was located at *T*1, and then used Monte Carlo simulations to infer octahedral occupancies from IR spectroscopy data. The two occupancy models used by these authors had Al at *M*2 and Al at *M*2 and *M*3; simulations gave better agreement for the latter. These diverse and sometimes contrasting results for both the octahedral and tetrahedral sites highlight the need for further investigation of this system.

It has been suggested that coupling between *M* and *T* sites is an important control on ordering in certain amphiboles. Hawthorne (1997) suggested that coupling occurs between Al at *M*2 and *T*1 on the grounds that if Al rather than Si is at *T*1, a more favourable bond-valence sum is incident at the O(1) atom. This theory is supported by the experimental results of Jenkins (1994), who studied a series of tremolite–tschermakite amphiboles and found that agreement between his experiment and activity-composition models was best for a model involving coupling between Al at *M*2 and *T*1. Subsequently, Welch *et al.* (1998) proposed that coupling between Al at *M*2 and *T*2

was a significant factor in controlling the long-range order behaviour of Al and Si in the tetrahedral sites. The simulation method we have employed in this work is capable of accounting for possible coupling terms, by including interactions between the tetrahedral and octahedral sites ($T-O$), as well as $T-T$ and $O-O$ interactions.

## Methods

The method we employed in this work is identical to that previously employed in our study of glaucophane (Palin *et al.*, 2003*b*). The general approach is described in detail elsewhere (Bosenick *et al.*, 2001; Warren *et al.*, 2001); here we simply note that it comprises two stages: firstly, lattice energy minimization methods are used to compute values for atomic interaction parameters and chemical potentials; and secondly, these values are used in Monte Carlo simulations of ordering. In this work, as for glaucophane, the atomic interaction parameters were determined using an empirical method, and a quantum mechanical approach was used to calculate the chemical potentials. The general expression for the ordering energy is

$$E = E_0 + \sum_i N^i_{\mathrm{Al-Al}} J_i + \sum_j \mu_j x^j_{\mathrm{Al}} \qquad (1)$$

where $E$ denotes the energy of a particular configuration of cations, $E_0$ denotes an energy constant subsuming all energy terms not involved in the ordering process, $J_i$ indicates the $i$th pair interaction parameter, and $N^i_{\mathrm{Al-Al}}$ denotes the number of Al−Al linkages corresponding to $J_i$ (the choice of atom type here is arbitrary, any of the atom types involved in ordering could be chosen). Where there is more than one type of site (e.g. tetrahedral *vs.* octahedral), a chemical potential $\mu_j$ can be included to express the preference of a cation for a particular site type $j$ (again we have chosen to compute chemical potentials with respect to Al; the value of the chemical potential is multiplied by $x_{\mathrm{Al}}$, the fraction of sites of type $j$ which are occupied by Al). Equation 1 is simply a multilinear regression problem; given a set of $N^i_{\mathrm{Al-Al}}$ and $E$ values, computer algorithms can be used to solve for $E_0$ and a set of $J$ values (and $\mu$ values, if used). The $E$ values are obtained by constructing a set of model configurations in which the cations of interest are randomly located across the sites which take part in ordering; each of these configurations is optimized using the lattice energy minimization program GULP to yield an $E$ value. For each configuration, the $N^i_{\mathrm{Al-Al}}$ values are determined by a spreadsheet method. The specific procedure is discussed below.

### *Interatomic potentials and model testing*

The tschermakite model consists of two parts: structural data (cell parameters and atomic coordinates), and a series of empirical interatomic potentials to model the interactions between the atoms. The parameters used in the interatomic potentials for the tschermakite model are given in Table 1. Four types of potential are employed, and two types of oxygen atom are considered: "O1" is used to denote oxygen atoms forming part of a hydroxyl group, and "O2" is used for all other oxygen atoms.

Buckingham potentials are used to model short-range interactions such as Si−O and K−O:

$$E(r) = A\ \exp(-r/\rho) - Cr^{-6} \qquad (2)$$

where $A$, $\rho$ and $C$ are adjustable parameters. When $C = 0$, as is the case for all short-range interactions except for Si−O2 and O−O, the functional form is that of the Born-Mayer potential.

The Morse potential is used to model the hydroxyl group (i.e. bonding between O1 and H):

$$E(r) = D[(1 - \exp[-a(r - r_0)])^2 - 1] \qquad (3)$$

where $D$, $a$, $r$ and $r_0$ are adjustable parameters. The polarizability of the oxygen atom is modelled via the core-shell potential, in which each oxygen atom is considered as a core consisting of the nucleus and inner electrons, and a massless shell consisting of the outer electrons. The core and shell are linked by an harmonic interaction, related to the displacement of the core with respect to the centre of the shell, $d$:

$$E(d) = \frac{1}{2}Kd^2 \qquad (4)$$

where $K$ is an adjustable parameter. Atoms comprising polyhedral units ($MgO_6$ and $AlO_6$ octahedra, and $AlO_4$ and $SiO_4$ tetrahedra) are held together by three-body potentials, which act against unrealistic distortions of the polyhedra, and are of the form

$$E(\theta) = \frac{1}{2}k(\theta - \theta_0)^2 \qquad (5)$$

TABLE 1. Parameters used in interatomic potentials (equations (2−5)).

| Type and species[a] | Parameter values | | | | Reference[b] |
|---|---|---|---|---|---|
| Buckingham: | $A$ (eV) | ρ (Å) | $C$ (eV Å$^{-6}$) | | |
| Si c − O1 c | 999.9 | 0.3012 | 0 | | 1 |
| Si c − O2 s | 1283.907 | 0.3205 | 10.66 | | 1 |
| Al c − O1 c | 1142.677 | 0.2991 | 0 | | 2 |
| Al c − O2 s | 1460.3 | 0.2991 | 0 | | 1 |
| O2 s − O2 s | 22764 | 0.149 | 27.88 | | 1 |
| O1 c − O2 s | 22764 | 0.149 | 27.88 | | 1[c] |
| O1 c − O1 c | 22764 | 0.149 | 27.88 | | 1[c] |
| H c − O2 s | 311.97 | 0.25 | 0 | | 1 |
| Mg c − O1 c | 1142.677 | 0.2945 | 0 | | 3 |
| Mg c − O2 s | 1428.5 | 0.2945 | 0 | | 1 |
| Ca c − O2 s | 2272.74 | 0.2986 | 0 | | 4 |
| Ca c − O1 c | 2272.74 | 0.2986 | 0 | | 4[c] |
| Spring (core-shell): | $K$ (eV Å$^{-2}$) | | | | |
| O2 c − O2 s | 74.92 | | | | 3 |
| Morse: | $D$ (eV) | α (Å$^{-1}$) | $r_0$ (Å) | $r_{max}$ (Å) | |
| O1 c − H c | 7.0525 | 2.1986 | 0.9485 | 1.4 | 1 |
| Three-body: | $k$ (eV rad$^{-2}$) | $\theta_0$ (°) | $r_{max}$(1−2) (Å)[d] | $r_{max}$(1−3) (Å) | |
| O − Si c − O[e] | 2.0974 | 109.47 | 1.8 | 3.2 | 1 |
| O − Al1 c − O | 2.0974 | 109.47 | 1.95 | 3.4 | 1[f] |
| O − Al2 c − O | 2.0974 | 90 | 2.2 | 3.2 | 1 |
| O − Mg c − O | 2.0974 | 90 | 2.2 | 3.2 | 3 |

[a] c = core, s = shell
[b] References: 1 − Winkler *et al.* (1991), 2 − Schröder *et al.* (1992), 3 − Sainz-Diaz *et al.* (2001), 4 − Bush *et al.* (1994)
[c] Assumed by analogy with similar potentials in specified reference
[d] $r_{max}$ (1−2) = $r_{max}$ (2−3)
[e] "O" denotes any oxygen atom (O1 or O2)
[f] $r_{max}$ values modified from potential in specified reference

where $k$ is an adjustable parameter, and $\theta_0$ is taken to be the ideal angle at the centre of the polyhedron (i.e. 90º for octahedral coordination and 109.47º for tetrahedral coordination).

Before proceeding with the calculation of any $J$ parameters, it is first necessary to create a disordered model of the system, from which a data set of configurations (and hence values for $E$ and $N^i_{Al-Al}$) can then be generated. Disorder is represented by assigning to each site available for ordering a virtual occupancy corresponding to the statistically-disordered (high-temperature) case; this is known as the 'virtual crystal approximation' (VCA). In the case of tschermakite, this means that all the tetrahedral sites are occupied by 0.25 Al and 0.75 Si, and all octahedral sites by 0.4 Al and 0.6 Mg. Since tschermakite is not a naturally-occurring mineral, no cell parameters were available for the initial model. Instead, the cell parameters were extrapolated back from experimental cell parameters for tremolite (Hawthorne *et al.*, 1997) and magnesiohornblende (Jenkins *et al.*, 1997), assuming a linear relationship between compositions (Vegard's Law). The initial atomic coordinates used were those for glaucophane. The model was optimized with GULP at constant pressure (i.e. allowing the cell parameters to change), using the potential parameters in Table 1. Whilst in this study the optimized structure cannot be compared with an experimentally-determined one, its cell parameters were sensible for calcic amphiboles, and visual inspection of the structure with Cerius[2] showed that the atoms were in feasible positions with correct coordinations.

### *Calculation of J values and chemical potentials*

As already specified above, this study investigates the effect of coupled ordering schemes (Al/Mg in the octahedra *vs.* Al/Si in the tetrahedra), and of the possible preference of Al for a particular type of site (*T*1/2, *M*1/2/3). It was thus necessary to use three sets of *J* values – namely for *T*–*T*, *O*–*O* and *T*–*O* interactions. The first stage of the process was to calculate a set of *T*–*T* interactions. Rather than calculating new *O*–*O* interactions, the values determined for glaucophane were used (Palin *et al.*, 2003*b*); these are reproduced in Table 2. The second stage was to combine these *O*–*O* interactions with the calculated *T*–*T* interactions to enable the evaluation of the *T*–*O* interactions. Chemical potentials were also determined, as discussed below.

The ordering behaviour of tremolite–tschermakite was examined by beginning from a model of end-member tschermakite, despite the fact that it does not occur naturally. The reason for this is that compositions in the naturally-occurring part of the solid solution cannot be used for this purpose – tremolite because all sites are occupied by one species only, giving no capacity for cation ordering; and magnesiohornblende because the tetrahedral occupancy is very dilute (Al:Si = 1:7), and would not result in a sufficient $N^{i}_{\mathrm{Al-Al}}$ database from which to calculate the $J_{T-T}$ parameters.

### *Calculation of T–T Js and chemical potential*

To calculate the *T*–*T* interactions, the optimized VCA model of tschermakite was used to generate a data set of 90 configurations, each with Al and Si atoms randomly located on the tetrahedral sites and the VCA employed for the octahedral sites, since the behaviour of the octahedral cations was not known. These configurations were each then optimized with GULP.

TABLE 2. Assigned *J* parameters (*O*–*O*) for glaucophane.

| Parameter | Distance (Å) | Type | Value (eV) |
|---|---|---|---|
| $J_1$ | 3.077 | Intra-ribbon | 0.60(3) |
| $J_2$ | 3.098 | Intra-ribbon | " |
| $J_3$ | 3.107 | Intra-ribbon | " |
| $J_4$ | 3.148 | Intra-ribbon | " |
| $J_5$ | 5.313 | Intra-ribbon | 0.20(3) |
| $J_6$ | 5.369 | Inter-ribbon | −0.02(5) |
| $J_7$ | 5.400 | Intra-ribbon | 0.23(4) |
| $J_8$ | 6.155 | Intra-ribbon | 0.21(4) |
| $J_9$ | 6.176 | Intra-ribbon | 0.21(3) |
| $J_{10}$ | 6.296 | Intra-ribbon | 0.20(11) |
| $J_{11}$ | 6.325 | Inter-ribbon | 0.02(5) |
| $J_{12}$ | 6.652 | Inter-ribbon | 0.01(5) |
| $J_{13}$ | 7.267 | Inter-ribbon | −0.01(5) |
| $J_{14}$ | 7.381 | Inter-ribbon | 0.01(2) |

Figures in brackets indicate the standard error on the final digit. Taken from Palin *et al.* (2003*b*).

The *T*–*T* interaction parameters were assigned by visual inspection of the tschermakite model using Cerius[2]. Interactions within the same double chain were considered; examples of these are shown in Fig. 2. In addition, interactions between sites in different double chains were included; these have been grouped according to the difference in the fractional *x* coordinates of two interacting sites, here labelled *w*. Figure 3 illustrates the groupings: interactions with $w = 0.59$ operate between tetrahedral sites in the same I beam, across the octahedral ribbon; $w = 0.41$ denotes interactions which operate between tetrahedra in I beams adjacent along *x*, and $w = 0.09$ shows interactions which operate between tetrahedra in I beams adjacent along *y*. Examples of the assigned *J*s for inter-chain interactions are shown in Figs 4 and 5.

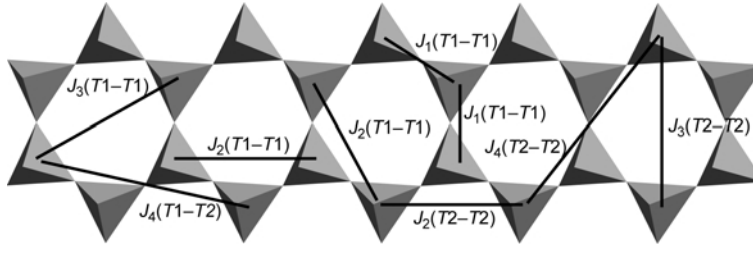


FIG. 2. Examples of distances corresponding to *J* parameters for tschermakite intra-chain *T*–*T* interactions.

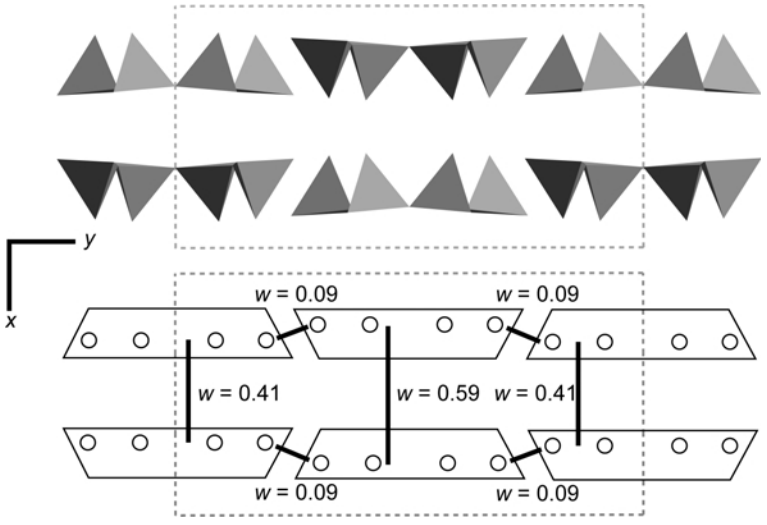


FIG. 3. End-on view of tetrahedral double chains in the tschermakite structure (top), with cartoon view (bottom) showing groupings of inter-chain $T-T$ interactions according to $w$, the difference in the fractional $x$-coordinates of interacting sites. Boxes indicate unit cells.

The distances over which all the $T-T$ interactions operate are given in Table 3. Initially, the $T1$ and $T2$ sites were considered separately; the interaction parameters calculated are given in Table 4*a*. However, as this table shows, the separate values for $J_1$ $T1-T1/J_1$

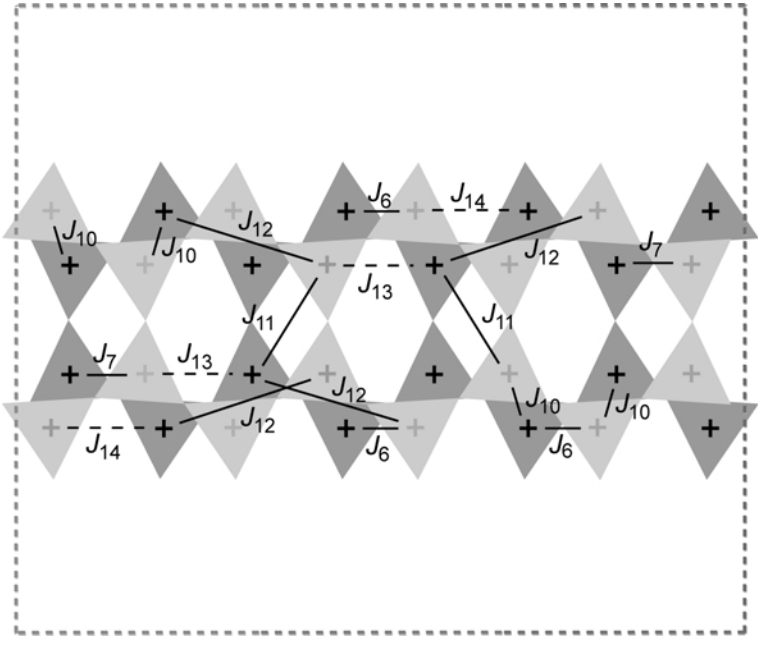


FIG. 4. Projection on (100) of selected tetrahedral sites in tschermakite, showing examples of distances corresponding to $J$ parameters for inter-chain $w = 0.41$ and $w = 0.59$ $T-T$ interactions. Solid lines correspond to interactions for which $w = 0.41$, dotted lines to interactions for which $w = 0.59$. The box indicates the unit cell.

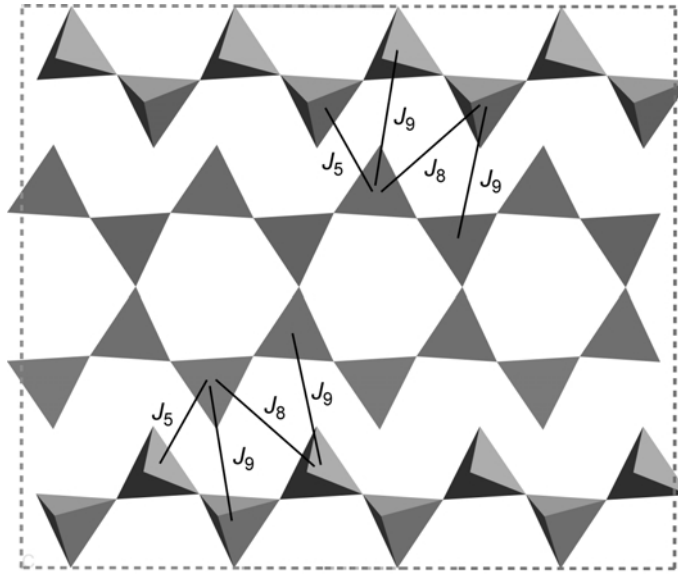


FIG. 5. Projection on (100) of selected tetrahedral sites in tschermakite, showing examples of distances corresponding to $J$ parameters for inter-chain $w = 0.09$ $T-T$ interactions. The box indicates the unit cell.

$T1-T2$, $J_2$ $T1-T1/J_2$ $T1-T2$, $J_3$ $T1-T1/J_3$ $T2-T2$ and $J_4$ $T1-T2/J_4$ $T2-T2$ were within error of one another. Hence, these values were considered together, and a new fit performed ($J_2$ $T2-T2$ was not within error of the other $J_2$ values, so it was still considered separately). The $J$ values resulting from this new fit are given in Table 4*b*.

The quality of the fit is shown in Fig. 6; the $R^2$ values are 0.956 for the initial model and 0.953 for the simplified model. This shows that the

TABLE 3. Distances corresponding to $T-T$ $J$ parameters for tschermakite.

| Parameter | Distance (Å) | Interacting sites | Type | $w$ |
|---|---|---|---|---|
| $J_1$ $T1-T1$ | 3.0653 | $T1-T1$ | Intra-chain | – |
| $J_1$ $T1-T2$ | 3.0565 & 3.1165 | $T1-T2$ | Intra-chain | – |
| $J_5$ | 3.5809 | $T2-T2$ | Inter-chain | 0.09 |
| $J_6$ $T2-T2$ | 3.9074 | $T2-T2$ | Inter-chain | 0.41 |
| $J_7$ $T1-T1$ | 4.058 | $T1-T1$ | Inter-chain | 0.41 |
| $J_8$ $T2-T2$ | 4.2459 | $T2-T2$ | Inter-chain | 0.09 |
| $J_9$ $T1-T2$ | 4.3855 | $T1-T2$ | Inter-chain | 0.09 |
| $J_{10}$ $T1-T2$ | 4.5425 | $T1-T2$ | Inter-chain | 0.41 |
| $J_{11}$ $T1-T1$ | 5.0856 | $T1-T1$ | Inter-chain | 0.41 |
| $J_2$ $T1-T1$ | 5.3171 | $T1-T1$ | Intra-chain | – |
| $J_2$ $T2-T2$ | 5.3171 | $T2-T2$ | Intra-chain | – |
| $J_2$ $T1-T2$ | 5.3236 & 5.3583 | $T1-T2$ | Intra-chain | – |
| $J_{12}$ $T1-T2$ | 5.4892 | $T1-T2$ | Inter-chain | 0.41 |
| $J_{13}$ $T1-T1$ | 5.5727 | $T1-T1$ | Inter-chain | 0.59 |
| $J_{14}$ $T2-T2$ | 5.7263 | $T2-T2$ | Inter-chain | 0.59 |
| $J_3$ $T1-T1$ | 6.1374 | $T1-T1$ | Intra-chain | – |
| $J_3$ $T2-T2$ | 6.198 | $T2-T2$ | Intra-chain | – |
| $J_4$ $T1-T2$ | 8.094 & 8.162 | $T1-T2$ | Intra-chain | – |
| $J_4$ $T2-T2$ | 8.166 | $T2-T2$ | Intra-chain | – |

TABLE 4. (*a*) *J* and μ values for initial model with separate consideration of *T*1 and *T*2 sites. (*b*) *J* and μ values for simpler model with some combination of *J*s with similar values

| (*a*) | | (*b*) | |
|---|---|---|---|
| Parameter | Value (eV) | Parameter | Value (eV) |
| $J_1$ $T1-T1$ | 1.05(9) | $J_1$ | 0.98(4) |
| $J_1$ $T1-T2$ | 0.96(4) | $J_2$ $T1-T1$,$T1-T2$ | 0.13(4) |
| $J_5$ | 0.24(8) | $J_2$ $T2-T2$ | 0.29(7) |
| $J_6$ | 0.28(7) | $J_3$ | 0.08(5) |
| $J_7$ | 0.03(8) | $J_4$ | 0.01(3) |
| $J_8$ | 0.16(7) | $J_5$ | 0.26(8) |
| $J_9$ | 0.19(5) | $J_6$ | 0.28(7) |
| $J_{10}$ | 0.32(5) | $J_7$ | 0.03(8) |
| $J_{11}$ | 0.21(8) | $J_8$ | 0.16(7) |
| $J_2$ $T1-T1$ | 0.09(6) | $J_9$ | 0.21(5) |
| $J_2$ $T2-T2$ | 0.30(8) | $J_{10}$ | 0.33(5) |
| $J_2$ $T1-T2$ | 0.16(4) | $J_{11}$ | 0.17(8) |
| $J_{12}$ | 0.25(6) | $J_{12}$ | 0.25(6) |
| $J_{13}$ | 0.45(8) | $J_{13}$ | 0.42(7) |
| $J_{14}$ | 0.38(8) | $J_{14}$ | 0.36(7) |
| $J_3$ $T1-T1$ | 0.15(7) | μ($T1$) | −0.50(7) |
| $J_3$ $T2-T2$ | 0.03(9) | | |
| $J_4$ $T1-T2$ | 0.00(4) | | |
| $J_4$ $T2-T2$ | 0.02(6) | | |
| μ($T1$) | −0.54(11) | | |

Figures in brackets represent the standard error on the final digit.

simplification does not affect the quality of the fit, so the second set of *J*s, from the simpler model, was used in all subsequent investigations. Additionally, both the sign and the magnitude of μ($T1$) are approximately the same in both fits.

### *Calculation of T−O Js and chemical potentials*

Having the calculated $T-T$ interaction parameters, the next stage of the process was to calculate the $T-O$ *J*s, so that a complete model of tschermakite could be constructed (using the

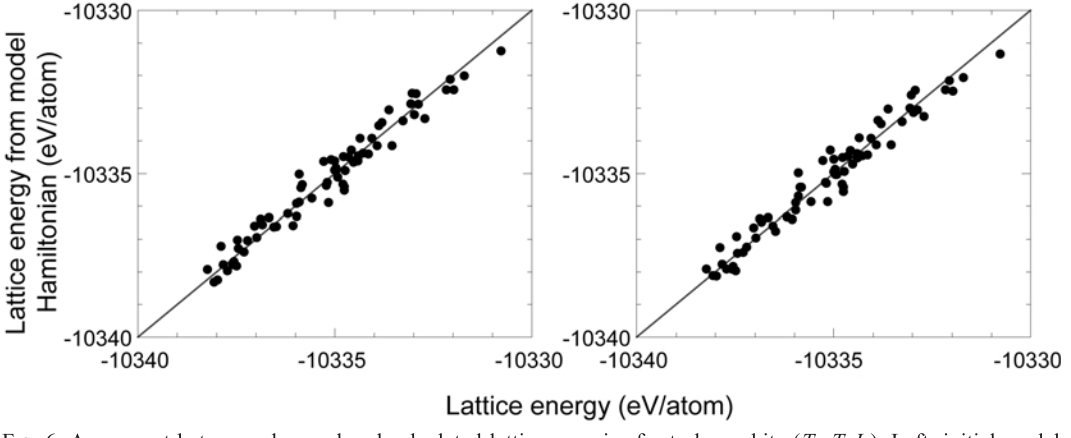


FIG. 6. Agreement between observed and calculated lattice energies for tschermakite ($T-T$ *J*s). Left: initial model ($R^2$ = 0.956), right: simplified model with combined *J* parameters ($R^2$ = 0.953). Straight lines indicate perfect agreement.

*O*−*O* *J*s from glaucophane). The set of *T*−*O* interactions (Table 5) was chosen so that it includes the nearest- and next-nearest *T*−*O* neighbours for all possible types of *T*−*O* interaction (i.e. all permutations between *T*1/*T*2 and *M*1/*M*2/*M*3). Nearest-neighbour *T*−*O* interactions are labelled $J_{1a}$, $J_{1b}$ etc.; next-nearest neighbour *T*−*O* interactions are labelled $J_b$, $J_c$ etc. Again, this encompasses interactions between sites in the same I beam, and between sites in different I beams (see Figs 7 and 8). The chemical potentials were chosen to be μ(*M*1), μ(*M*2) and μ(*T*1); only three chemical potentials are required. In general, if there are *n* types of site across which ordering can occur, there are *n*−1 independent chemical potentials. In tschermakite, there are five site types, but there are three chemical potentials, not four: exchange of Si and Mg between the tetrahedral and octahedral sites is not expected in amphiboles, and this effectively adds a further constraint to the chemical potentials. To put it another way, there are three octahedral site types, leading to two independent octahedral chemical potentials, and two tetrahedral site types, leading to one independent tetrahedral chemical potential.

For the calculation of the T−*O* *J*s, a new data set of 90 configurations was generated, with Al and Si randomly located across the tetrahedral sites and Al and Mg randomly located across the octahedral sites. The VCA can no longer be used for the octahedral sites since interactions are now being counted between octahedra and tetrahedra; octahedral occupancy did not affect the previous count of interactions between tetrahedra only. The inclusion of a new set of configurations also effectively increases the size of the overall data set used, since overall there is a large number of fitted parameters and the number of configurations should be considerably larger than the number of parameters. The fit included all the *T*−*T* *J*s (using the simplified set from Table 4*b*), all the *O*−*O* *J*s from glaucophane, and the *T*−*O*

TABLE 5. Distances corresponding to *T*−*O* *J*s.

| Parameter | Distance (Å) | Type |
|---|---|---|
| $J_{1a}$ | 3.18 | *T*1−*M*3, same I beam |
| $J_{1b}$ | 3.185 | *T*1−*M*1, same I beam |
| $J_{1c}$ | 3.216 | *T*1−*M*2, same I beam |
| $J_{1d}$ | 3.217 | *T*2−*M*1, same I beam |
| $J_{1e}$ | 3.222 | *T*2−*M*2, same I beam |
| $J_b$ | 3.327 | *T*2−*M*2, different I beams |
| $J_c$ | 4.42 | *T*1−*M*1, same I beam |
| $J_{1f}$ | 4.47 | *T*2−*M*3, same I beam |
| $J_d$ | 5.123 | *T*2−*M*1, different I beams |
| $J_e$ | 5.182 | *T*1−*M*2, different I beams |
| $J_f$ | 5.384 | *T*1−*M*3, same I beam |
| $J_g$ | 5.455 | *T*2−*M*3, same I beam |

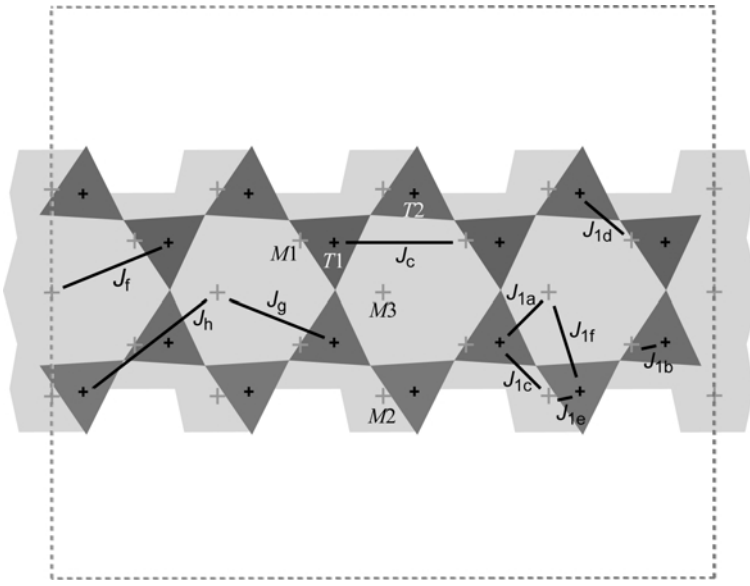


FIG. 7. Examples of distances corresponding to *T*−O *J* parameters between sites in the same I beam. The tetrahedral double chain is shown in dark grey and an adjacent octahedral ribbon in light grey; the box indicates the unit cell.

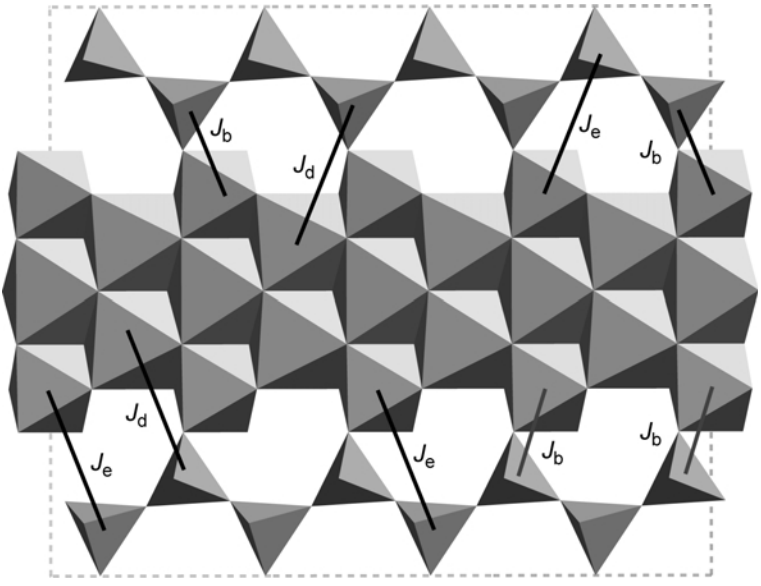


FIG. 8. Examples of distances corresponding to $T-O$ $J$ parameters between sites in different I beams. The unit cell is indicated by the box.

$J$s shown in Figs 7 and 8. Although all parameters were included in the fit, only the $T-O$ interactions and the chemical potentials were allowed to vary (as well as the $E_0$ value).

The set of $T-O$ $J$s and chemical potentials obtained by this fitting procedure is given in Table 6, and the $R^2$ value for this fit was 0.83. The nearest-neighbour interactions are all large and negative, implying favourable Al–Al interactions across such distances.

TABLE 6. $T-O$ $J$ and μ values as calculated from GULP.

| Parameter | Value (eV) |
|---|---|
| $J_{1a}$ | −0.6(2) |
| $J_{1b}$ | −0.4(2) |
| $J_{1c}$ | −0.4(2) |
| $J_{1d}$ | −0.7(1) |
| $J_{1e}$ | −0.4(2) |
| $J_b$ | −0.5(2) |
| $J_c$ | −0.1(2) |
| $J_{1f}$ | −0.3(2) |
| $J_d$ | −0.1(2) |
| $J_e$ | 0.1(2) |
| $J_f$ | 0.0(2) |
| $J_g$ | 0.0(2) |
| μ($M1$) | 0.0(4) |
| μ($M2$) | −0.3(5) |
| μ($T1$) | −0.8(3) |

Figures in brackets represent the standard error on the final digit.

### *SIESTA calculations*

In our previous study of glaucophane, we found that there was a discrepancy between the chemical potentials that were calculated via the empirical method (GULP) and those calculated using the *ab initio* code SIESTA. In some respects this was a little surprising, because we had anticipated that the empirical models would be capable of handling the energetics of ordering between chemically-similar sites (unlike the case where cations order between sites of different coordination number). Therefore, in the present study we tested our empirical models on this point by calculating chemical potentials for the tschermakite system, using both empirical and *ab initio* methods following the approach used in our study of glaucophane.

For the SIESTA calculations, eight ordered configurations were produced, and optimized. As was the case with glaucophane, the configurations were chosen so that they were significantly different from one another in an attempt to compensate for the small number of configurations. Four of them had Al on $T1$, and four had Al

on *T*2; for each set of four, the octahedral Al was incorporated on either *M*1, *M*2, ½*M*2 + *M*3, or ½*M*1 + *M*3. The pseudopotentials used were produced for other systems: Mg from MgO and Si from solid silicon (Anglada *et al.*, 2002), Al from alumina, Ca from calcite, and O and H from water simulations (all unpublished data). The basis sets were DZP in each case, with semi-core states included for the Ca atoms, and calculations were performed with the generalized gradients approximation (GGA).

The procedure for determining the chemical potentials is as follows. Consider the separate contributions to the energy – namely, the constant part of the energy not involved in cation ordering, $E_0$, which is the first term in equation 1; the energy due to the *J*s, $E_J$, which corresponds to the second term in equation 1; and the energy due to the chemical potentials, $E_\mu$, which corresponds to the third term in equation 1. Using subscripts G and S for GULP and SIESTA, the energies can then be written as

$$E_G = E_0 + E_J + E_\mu \quad (6)$$
$$E_S = E_0' + E_J + E_\mu' \quad (7)$$

where the prime symbols indicate that the difference between an energy calculated from GULP and one calculated from SIESTA is due to differences in $E_0$ and $E_\mu$. Thus, for each configuration, the exchange energies, computed from the *J* and $N^i_{Al-Al}$ values, were subtracted from the energies of the eight relaxed structures calculated using SIESTA:

$$E_S - E_J = E_0' - E_\mu' \quad (8)$$

This equation was manipulated by linear regression, as before – for each of the eight configurations, the values of μ(*T*1), μ(*M*1) and μ(*M*2) (which contribute to $E_\mu'$) and $E_0'$ were fitted against the values of $E_S - E_J$. The chemical potentials thus obtained are given in Table 7. These were used, together with the *J*s obtained from GULP, to compute the new calculated energies, which were then compared with the *E* values obtained from GULP. This comparison is shown in Fig. 9, the correlation coefficient $R^2$, is 0.81.

TABLE 7. Chemical potentials for tschermakite, calculated using SIESTA.

| Parameter | Value (eV) |
|---|---|
| μ(*M*1) | −0.2(2) |
| μ(*M*2) | −0.3(2) |
| μ(*T*1) | −0.7(1) |

As it happens, the μ values obtained from SIESTA are not too different from those calculated with GULP (hence the similar $R^2$ values, 0.83 and 0.81). Contributions to the chemical potentials from elastic (strain) effects and those from bonding effects can have different degrees of significance in different systems, the former being modelled well by GULP and the latter being modelled well by SIESTA. Where the agreement between the two methods is high, one can infer that the tschermakite chemical potentials are mostly due to strain (size-related effects).

Finally, as was the case for glaucophane, it should be noted that the energy contribution from the *J* values is of the same order of magnitude as that from the chemical potentials, so the behaviour of the system cannot simply be predicted from the *J* values or chemical potentials alone; both contributions must be included.

### *Monte Carlo simulations*

The procedure employed in the Monte Carlo (MC) simulations is explained in detail in an earlier review paper (Warren *et al.*, 2001). The program used to perform the simulations is OSSIA, see http://www.esc.cam.ac.uk/ossia for details. We will not consider the details of the MC simulation process here, but we note that for the

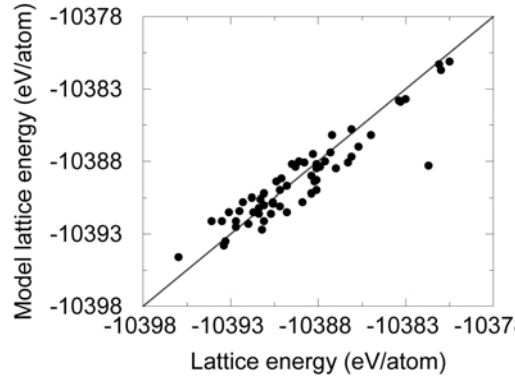


FIG. 9. Agreement between observed (GULP) and calculated lattice energies (model Hamiltonian, using chemical potentials from SIESTA) for the whole-cell tschermakite model. The straight line indicates perfect agreement. The correlation coefficient $R^2$ for this model is 0.81.

purposes of the MC simulations, it is more convenient to express the energy of the system in the following form:

$$E = \sum_{\langle i,j \rangle} J_{ij} S_i S_j + \sum_j \mu_j S_j \qquad (9)$$

In equation 9, the quantity $S$ denotes a site variable which is defined to be 1 if the site is occupied by Al and zero otherwise. $J_{ij}$ is the interaction parameter between site $i$ and site $j$, with the angle brackets <···> denoting that no interaction is counted twice, and $\mu_j$ is the chemical potential associated with a particular site $j$. Equation 9 is thus equivalent to equation 1, with the omission of the constant term $E_0$, which does not affect the ordering process and therefore does not need to be included in the MC simulations. Implicit in this formalism is the representation of the system of interest as a set of spins interacting with a specified connectivity and specified energies of interaction (the $J$ parameters); these spins are then mapped onto a crystal structure at the end of the simulation.

OSSIA can output the thermodynamic averages of the energy $E$ and order parameter $Q$ of the system at a particular temperature, together with the mean squared values $E^2$ and $Q^2$. These quantities are useful since they allow direct calculation of the heat capacity $C$ and susceptibility $\chi$ of the system:

$$\chi = \frac{\langle Q^2 \rangle - \langle Q \rangle^2}{k_B T} \qquad (10)$$

$$C = \frac{\langle E^2 \rangle - \langle E \rangle^2}{k_B T^2} \qquad (11)$$

At a phase transition, there will be anomalies in both the heat capacity and susceptibility, thereby enabling one to determine whether or not a system exhibits a phase transition by examining the simulation data.

In this work, we have performed several MC simulations for tschermakite. The first simulation is of one isolated tetrahedral double chain, excluding interactions with other chains. This system is interesting because it can be considered as a quasi-1D system, and it is a well known result that 1D systems do not exhibit phase transitions.

The second simulation is of interacting tetrahedral double chains. This increases the dimensionality of the system. Our interest here is in investigating whether interacting chains will still order in the same pattern as the non-interacting chain, and whether the inter-chain interactions constrain the order in one chain with respect to that in the next. Previous work on muscovite (Palin *et al.*, 2001) suggested that ordering within one sheet of tetrahedrally coordinated cations occurred independently of neighbouring sheets – interactions between sheets were much weaker than those within sheets. One might expect the quasi-1D tetrahedral chain to show different behaviour from the muscovite sheet, which is effectively two-dimensional.

Finally, the whole set of calculated parameters is combined, and whole-cell simulations performed. This is a realistic model of the behaviour of the whole system, and it should give several insights – whether the $T$–$O$ interactions affect the ordering seen in the tetrahedral sheet; if so, what the nature of the new ordering behaviour is; whether the system undergoes any phase transitions; and whether any comparisons can be drawn with experimentally observed behaviour. A final whole-cell simulation is performed for magnesiohornblende, in order to investigate any differences between its overall behaviour and that of tschermakite.

## Results

### *Monte Carlo simulations of tschermakite*

#### *Simulation of an isolated tetrahedral double chain*

Since the tetrahedral double chain is a quasi-1D system, we performed some MC simulations of simpler chains, in order to draw comparisons with the real system. These simulations were of chains based on a square lattice, with varying widths $W$ (see Fig. 10). A 1:1 ratio of atoms was used, and interactions were defined only between nearest-

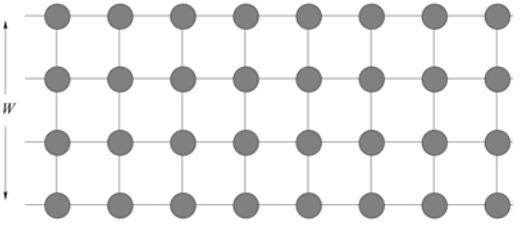


FIG. 10. Example of a quasi-1D system – a chain with width $W$ ($W$ = 4 in this example), based on a square lattice, with periodic boundary conditions governing its length, but not its width. Interacting sites are joined by solid lines.

neighbour atoms. The results for the 1D case (i.e. $W = 1$) and for $W = 2, 3, 4, 8$ are shown in Fig. 11; it can be seen from these results that there is no phase transition in the 1D system, nor in any of the quasi-1D systems – although the rapid drop to zero of the order parameter suggests that phase transitions occur, the heat capacity graphs are characteristic broad, asymmetric peaks ('Schottky anomalies'), not the divergent peaks one would associate with a phase transition. Results for a 2D simulation (i.e. $W = 1$) are also shown in Fig. 11; the sharper heat capacity anomaly is clearly visible. The results for the 1D and 2D systems are in exact agreement with the well-known theoretical results for 1D and 2D Ising models.

The tetrahedral double chain is topologically similar to the $W = 2$ case, but with every other cross-link missing. The two systems are not identical because only one $J$ value (that for nearest neighbours) was used in the $W = 2$ case, whilst the simulation of the real system used the first five $J$ values (i.e. all the intra-chain interactions), and $\mu(T1)$ from Table 4*b*. Furthermore, the composition of the double chain was that of tschermakite, i.e. Al:Si = 1:3, and not 1:1 as in the test cases. The double chain simulation results for the heat capacity show two Schottky peaks superimposed on one another, but no anomaly corresponding to a phase transition. Representative examples of the chain configurations at different temperatures are shown in Fig. 12, and for further clarification, Fig. 13 shows the evolution of the numbers of each type of interaction as a function of temperature, together with the heat capacity profile. These figures show that at the lowest temperatures, all

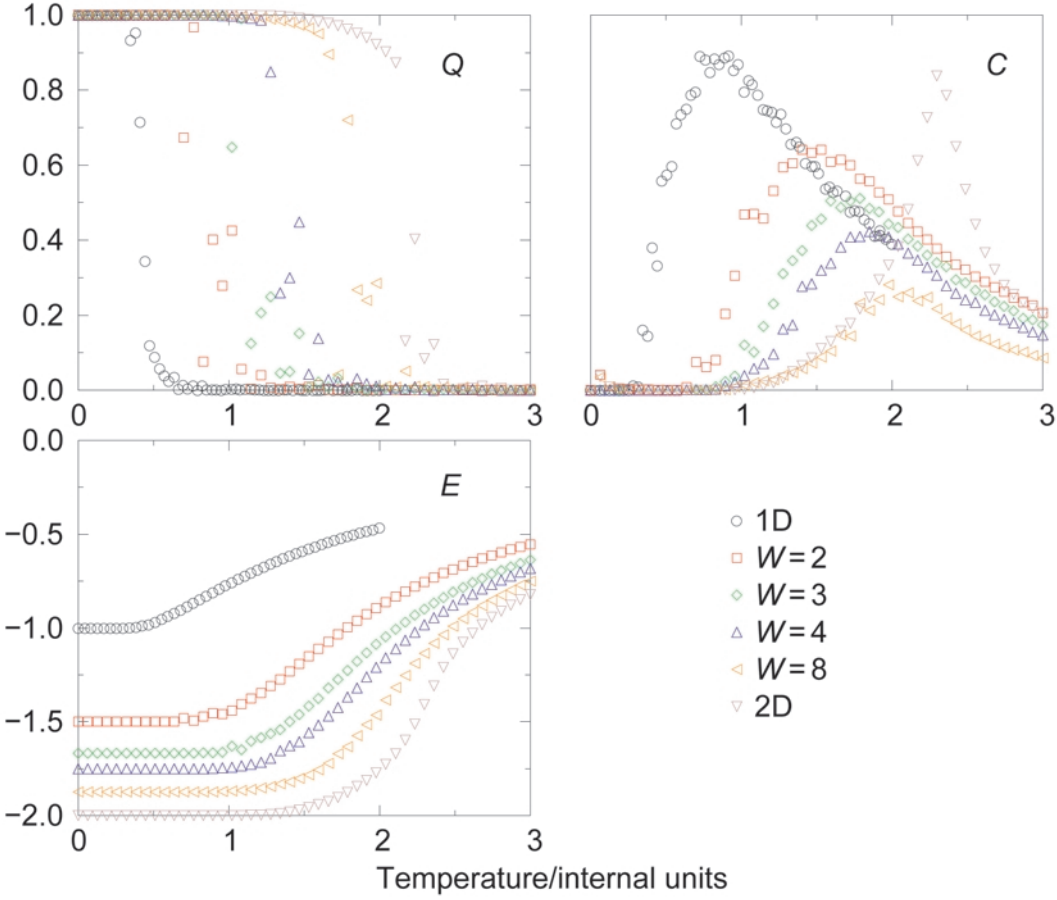


FIG. 11. MC simulation results for simple square-lattice-based chains such as that in Fig. 10. Order parameter ($Q$), heat capacity ($C$) and energy ($E$) results are shown.

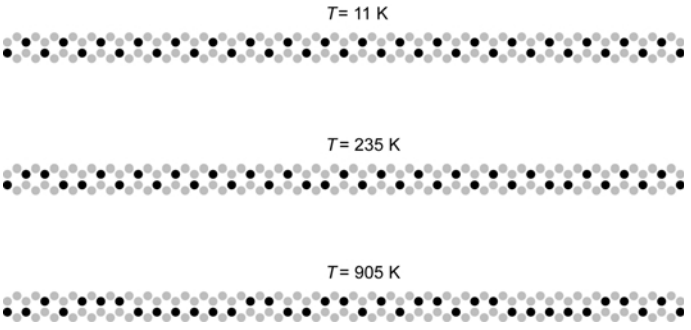


FIG. 12. Simulated structure of one tetrahedral double chain at various temperatures. Grey = Si, black = Al.

Al occurs on the $T1$ sites, interacting via $J_3$ interactions. This gives rise to a "para" arrangement of Al atoms. At slightly higher temperatures, Fig. 12 shows that some $J_2$ interactions begin to occur, giving rise to some 'meta' configurations; there are considerable numbers of 'meta' configurations as $T$ increases. The 'meta' configurations result in an increase in the energy, however, which is a less favourable situation than the 100% 'para' configuration. The presence of both configurations is consistent with NMR measurements of pargasite (Welch *et al.*, 1998), which has the same Al:Si ratio as that simulated.

Visual examination of the configurations in Fig. 12 suggests that the first Schottky peak in Fig. 13 corresponds to the formation of $J_2$ linkages (and hence the generation of some 'meta' configurations); it is somewhat less straightforward to determine the origin of the second, broader Schottky peak.

*Simulations of a system of interacting tetrahedral double chains*

The next stage of the investigation was to include the interactions between tetrahedral double chains. Hence, this simulation included all the $J$s and $\mu(T1)$ in Table 4*b*. In this system, a phase transition occurs, with Al atoms ordering onto $T1$ sites, interacting via $J_3$ interactions (the "para" configuration mentioned above). Figure 14 shows the sudden changes in the numbers of certain interactions – at low $T$ all the intra-chain Al interactions are $J_3$ , but a sudden decrease in $nJ_3$ (and corresponding sudden increase in $nJ_2(T1-T1,T1-T2)$) can be seen with increasing $T$.

The low-temperature ordering within one chain in a simulation with interacting tetrahedral double chains is therefore the same as that in a simulation of just one tetrahedral double chain, although the isolated chain simulation has no phase transition and the interacting chains do. The similarly-

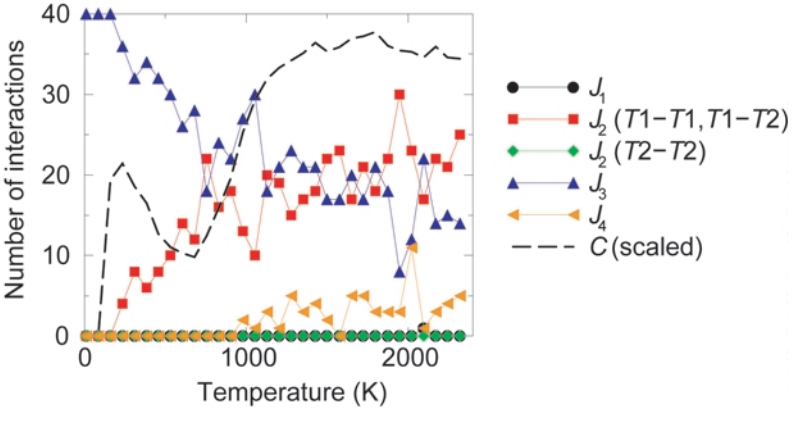


FIG. 13. Plot of number of interactions of various types as a function of temperature, for a simulation of an isolated tetrahedral double chain. The heat capacity profile is also shown.

ordered structures do not imply that the inter-chain interactions are insignificant; in fact, the converse is true: most of the inter-chain parameters are large and positive, so they are energetically not favoured. This is reflected in the *nJ* plot in Fig. 14 which shows the occurrences of most of the inter-chain interactions decreasing to zero with decreasing *T*. Conversely, the smallest of the inter-chain parameters is $J_7$, and this is manifested by an increase in the number of $J_7$ interactions with decreasing *T*. Inspection with Cerius[2] of the ordered state reveals that the ordering in each I beam does line up with respect to that in the next, with Al atoms interacting by means of $J_7$ interactions. $J_7$ is a $T1-T1$ interaction between I beams; a straight line drawn between the two interacting $T1$ sites is approximately equidistant from three "*A*" sites (which are vacant in these structures), yet all the other inter-I-beam interactions are unfavourable. It is clear from the values of $J_{13}$ and $J_{14}$ that interactions between tetrahedral sites in different chains but the same I beam are unfavourable, an interesting fact given that these sites are separated by the octahedral ribbon. These facts all illustrate that there are many complicated controls on the behaviour.

### *Whole-cell simulations*

The final simulations on tschermakite included the $T-T$ interactions from Table 4*b*, the $T-O$ interactions from Table 5 and the $O-O$ interactions from glaucophane (Table 2). The chemical potentials used were those from Table 7.

The simulation results indicate that there is no ordering phase transition in tschermakite – the heat capacity profile shows a straightforward Schottky anomaly (and is not illustrated for this reason). Figure 15*a* shows the evolution of the number of certain *J*s of various types as a function of temperature; all of these *J*s show a continuous change with temperature. Also shown is a plot of the Al site occupancies as a function of temperature (Fig. 15*b*). These occupancies are derived from order parameter variations in the simulation; the plot shows that there is little variation. These site occupancies suggest an Al preference for the $T1$ site over the $T2$ site ($T1:T2 \approx 60:40$) and for the $M2$ site over the $M1$ and $M3$ sites ($M1:M2:M3 \approx 30:60:10$).

### *Monte Carlo simulations of magnesiohornblende*

In the whole-cell MC simulation of magnesiohornblende, the *J* and μ values used were the same as those for the tschermakite whole-cell simulations, with the only difference between the two simulations being the compositions.

In contrast with the tschermakite simulations, the changes in the *nJ* plot (Fig. 16*a*) for magnesiohornblende are somewhat more obvious. In particular, the numbers of $J_2$ ($T1-T1$, $T1-T2$) and $J_3$ linkages are high at high temperature, but drop to zero as *T* decreases. The numbers of $O-O$ interactions can also be seen to diverge at T ≈ 1700 K, where e.g. the $J_{1-4}$ ($O-O$) interactions are increasing in number and the $J_5$ ($O-O$) interactions are decreasing in number. In spite of these changes in the *nJ* plot, this probably does not indicate a phase transition – the changes are not discontinuous, and visual

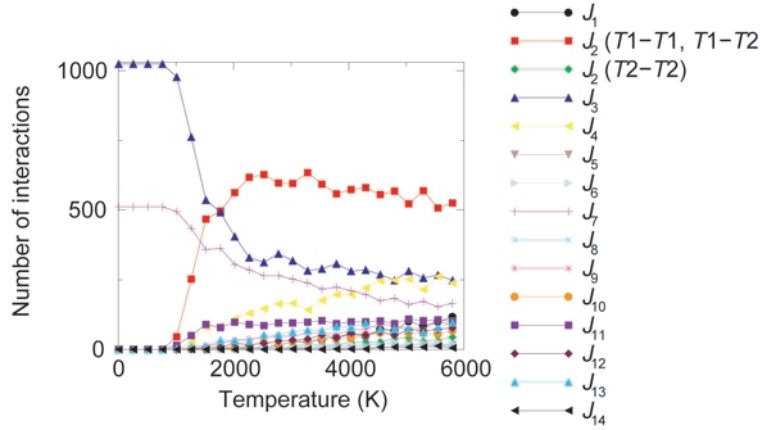


FIG. 14. Plot of number of interactions as a function of temperature, for a simulation of interacting tetrahedral double chains.

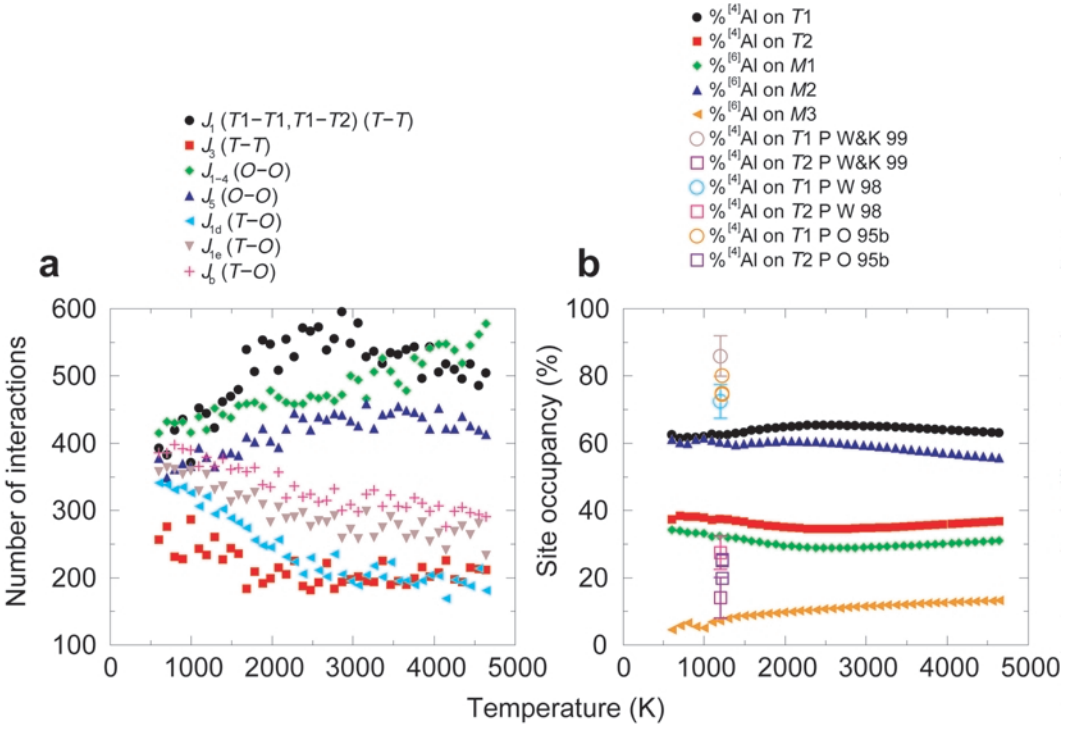


FIG. 15. (*a*) Evolution of numbers of selected interactions with temperature in the tschermakite whole-cell simulation. (*b*) Evolution of tschermakite Al site occupancies with temperature and comparison with values determined from experiment for minerals with similar tetrahedral and/or octahedral compositions (open symbols – symbol used for a particular experimental parameter is the same as that for the corresponding simulated parameter). Key to legend: P = pargasite; W&K 99 = Welch and Knight (1999), W 98 = Welch *et al.* (1998), O 95 b = Oberti *et al.* (1995*b*).

examination of randomly-selected ribbons of tetrahedra and octahedra shows a small amount of short-range order and occasional medium-range order, but no long-range order. Moreover, the heat capacity anomaly for magnesiohornblende is not dissimilar from that in tschermakite (not illustrated for this reason), where there was definitely no phase transition.

The Al site occupancy plot (Fig. 16*b*) shows that over experimentally-viable temperatures (i.e. <2000 K), the simulated Al site occupancy of the *M*2 site is ~60%, and that of the *T*1 site is ~70–80%. There is also a significant amount of Al at *M*1 (~30%).

## Discussion

The aluminous tremolite model formulated here is the most complex model that we have studied, with a total of 38 *J* values and three chemical potentials. Both whole-cell simulations suggest an Al preference for *T*1 over *T*2, and for *M*2 over *M*1 and *M*3. It is not possible to compare the tschermakite results with experiments, since tschermakite is a fictive end-member, not realized as a macroscopic phase in nature or experiment. However, experiments on magnesiohornblendes are in agreement with this simulated *T*1 preference. The consistency with experimental data is not as clear for octahedral sites. Experimental studies of $^{[6]}$Al occupancy have always concluded that Al should occur at *M*2, but the issue of *M*1/*M*3 occupancy has been somewhat more difficult to resolve, with more recent studies concluding that Al can occur at *M*3 but not *M*1. Our simulations show Al at *M*2 in accordance with experiment, but the fact that the *M*1 component (~30%) is larger than that at *M*3 (~15%) is at odds with experimental findings. It is not clear from this work why this is the case, as the quality of the fit for the whole-cell model (Fig. 9) was high, with $R^2$ = 0.81. The results

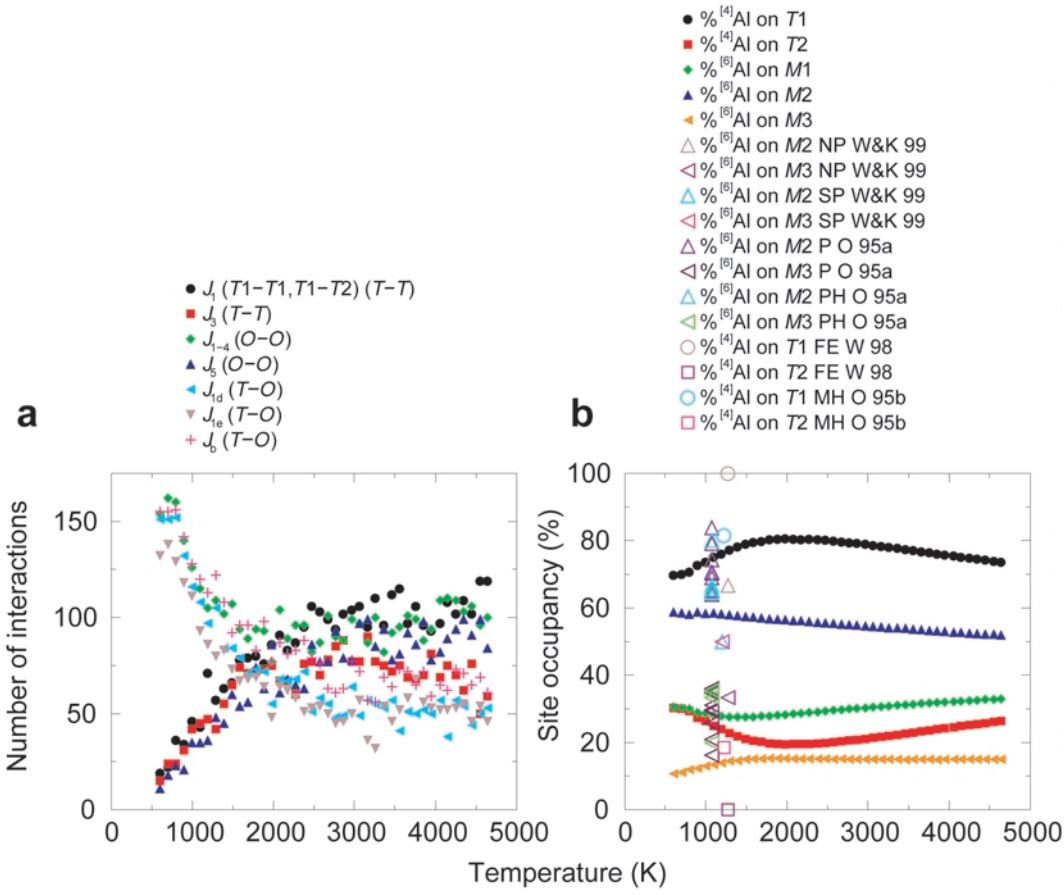


FIG. 16. (*a*) Evolution of numbers of selected interactions with temperature in the magnesiohornblende whole-cell simulation. (*b*) Evolution of magnesiohornblende Al site occupancies with temperature and comparison with values determined from experiment for minerals with similar tetrahedral and/or octahedral compositions (open symbols – symbol used for a particular experimental parameter is the same as that for the corresponding simulated parameter). Key to legend: NP = natural pargasite, SP = synthetic pargasite, P = pargasite, PH = pargasitic hornblende, FE = fluoredenite, MH = magnesiohornblende; W&K 99 = Welch and Knight (1999), W 98 = Welch *et al.* (1998), O 95a = Oberti *et al.* (1995*a*), O 95b = Oberti *et al.* (1995*b*).

presented here suggest that further study of these minerals may be necessary in order to rationalize their behaviour.

At first sight, the significant (20–30%) $^{[4]}$Al at *T*2 in magnesiohornblende is unexpectedly high. However, minor Al at *T*2 occurs in some high-temperature, Al-rich calcic and sodic-calcic amphiboles. A $^{29}$Si MAS NMR study (Welch *et al.*, 1998) of tetrahedral ordering in calcic and sodic-calcic amphiboles considered fluoredenite, a sodic-calcic amphibole with the same tetrahedral Al:Si ratio as magnesiohornblende, and concluded that all Al occurred at *T*1. However, pargasite, with the same tetrahedral Al:Si ratio as tschermakite, was also studied; in contrast to fluoredenite, it was concluded that pargasite had as much as 0.55 Al per formula unit (i.e. just over 25% of the total $^{[4]}$Al) at *T*2. The latter result was surprising, being unlikely on bond-valence grounds (Hawthorne, 1997), but confirmed later by neutron powder diffraction experiments (Welch and Knight, 1999). A suggested rationalization of this situation was that in pargasite, at high temperatures, distortions can occur around the O(4) atom (which is more underbonded if *T*2 = Al than if *T*2 = Si). Such distortions would allow a higher valence sum to be incident at O(4). Fluoredenite, on the other hand, has only Mg on

the *M* sites, and these divalent cations will result in a lower bond valence sum at O(4) than in pargasite, so that, even at high temperatures, it is not possible to accommodate such a low sum.

A final noteworthy result of these simulations is that the *T*−*O* interactions in aluminous tremolites are shown to be important. They are of the same order of magnitude as the nearest-neighbour *T*−*T* and *O*−*O* interactions, and this supports the suggestion that coupling between Al in the octahedra and tetrahedra is at least as important in controlling ordering as are the *T*−*T* and *O*−*O* couplings. All the nearest-neighbour *T*−*O* interactions are negative, implying favourable Al−Al coupling between tetrahedra and octahedra. The correlated errors on the values unfortunately do not permit the singling out of any specific *T*−*O* coupling as being more important than others.

## Conclusions

This paper has discussed the application of a computer simulation approach to studying the behaviour of complex amphiboles. The complex model we have formulated incorporates a large number of variables. Simulations of an isolated tetrahedral double chain yielded interesting results with respect to the dimensionality of the system. The extension of the model to a system of interacting tetrahedral double chains produced different thermodynamic behaviour, but the same intra-chain cation distribution at low temperatures, which demonstrates the complexity of the controls on the ordering behaviour of the system. Finally a whole-cell model was simulated, with interactions between tetrahedra, interactions between octahedra and interactions between the two. Neither the tschermakite nor the magnesiohornblende compositions exhibited a phase transition. Additionally, the simulation of interacting chains exhibits a phase transition, while the whole-cell model does not – this shows that the incorporation of *T*−*O* interactions results in different behaviour from that observed in *T*-only and *O*-only simulations. We also observed this phenomenon in our study of Al/Mg and Al/Si ordering in phengite (Palin *et al.*, 2003*a*).

By considering whole-cell simulations of aluminous tremolites, we have shown some simulation results for magnesiohornblende which compare reasonably well with experimental results from real samples. A particular advantage of this work is that it has been possible to model the site occupancies for each crystallographic site, which is difficult to achieve by experiment, and there was reasonable agreement at experimentally-viable temperatures between most of the magnesiohornblende site occupancies and corresponding values from experiment.

## Acknowledgements

EJP is grateful to Dr William Lee for fruitful discussions, to Mariví Fernández-Serra, Tom Archer and Andrew Walkingshaw for SIESTA assistance, and to EPSRC for financial support. The Monte Carlo simulations were performed on the Cambridge-Cranfield High Performance Computing Facility (CCHPCF) and on the Mineral Physics Group's Linux cluster. The SIESTA calculations were performed on the CCHPCF.

## References

Anglada, E., Soler, J.M., Junquera, J. and Artacho, E. (2002) Systematic generation of finite-range atomic basis sets for linear-scaling calculations. *Physical Review B*, **66**, art. no 205101.

Bosenick, A., Dove, M.T., Myers, E.R., Palin, E.J., Sainz-Diaz, C.I., Guiton, B., Warren, M.C., Craig, M.S. and Redfern, S.A.T. (2001) Computational methods for the study of energies of cation distributions: applications to cation-ordering phase transitions and solid solutions. *Mineralogical Magazine*, **65**, 193–219.

Bush, T.S., Gale, J.D., Catlow, C.R.A. and Battle, P.D. (1994) Self-consistent interatomic potentials for the simulation of binary and ternary oxides. *Journal of Materials Chemistry*, **4**, 831–837.

Della Ventura, G., Hawthorne, F.C., Robert, J.-L., Delbove, F., Welch, M. D. and Raudsepp, M. (1999) Short-range order of cations in synthetic amphiboles along the richterite-pargasite join. *European Journal of Mineralogy*, **11**, 79–94.

Hawthorne, F.C. (1981) Crystal chemistry of the amphiboles. Pp. 1–102 in: *Amphiboles and other Hydrous Pyriboles – Mineralogy* (D.R. Veblen, editor). Reviews in Mineralogy, **9A**. Mineralogical Society of America, Washington, D.C.

Hawthorne, F.C. (1983) The crystal chemistry of the amphiboles. *The Canadian Mineralogist*, **21**, 173–480.

Hawthorne, F.C. (1997) Short-range order in amphiboles: a bond-valence approach. *The Canadian Mineralogist*, **35**, 201–216.

Hawthorne, F.C., Della Ventura, G., Robert, J.-L., Welch, M.D., Raudsepp, M. and Jenkins, D.M. (1997) A Rietveld and infrared study of synthetic

amphiboles along the potassium-richterite-tremolite join. *American Mineralogist*, **82**, 708–716.

Hawthorne, F.C., Welch, M.D., Della Ventura, G., Liu, S., Robert, J.-L. and Jenkins, D.M. (2000) Short-range order in synthetic aluminous tremolites: an infrared and triple-quantum MAS NMR study. *American Mineralogist*, **85**, 1716–1724.

Jenkins, D.M. (1994) Experimental reversal of the aluminum content in tremolitic amphiboles in the system $H_2O$-CaO-MgO-$Al_2O_3$-$SiO_2$. *American Journal of Science*, **294**, 593–620.

Jenkins, D.M., Sherriff, B.L., Cramer, J. and Xu, Z. (1997) Al, Si, Mg occupancies in tetrahedrally and octahedrally coordinated sites in synthetic aluminous tremolite. *American Mineralogist*, **82**, 280–290.

Najorka, J. and Gottschalk, M. (2003) Crystal chemistry of tremolite-tschermakite solid solutions. *Physics and Chemistry of Minerals*, **30**, 108–124.

Oberti, R., Hawthorne, F.C., Ungaretti, L. and Canillo, E. (1995*a*) $^{VI}$Al disorder in amphiboles from mantle peridotites. *The Canadian Mineralogist*, **33**, 867–878.

Oberti, R., Ungaretti, L., Cannillo, E., Hawthorne, F.C. and Memmi, I. (1995*b*) Temperature-dependent Al order-disorder in the tetrahedral double chain of *C*2/*m* amphiboles. *European Journal of Mineralogy*, **7**, 1049–1063.

Palin, E.J., Dove, M.T., Redfern, S.A.T., Bosenick, A., Sainz-Diaz, C.I. and Warren M.C. (2001) Computational study of tetrahedral Al-Si ordering in muscovite. *Physics and Chemistry of Minerals*, **28**, 534–544.

Palin, E.J., Dove, M.T., Redfern, S.A.T., Sainz-Diaz, C.I. and Lee W.T. (2003*a*) Computational study of tetrahedral Al-Si and octahedral Al-Mg ordering in phengite. *Physics and Chemistry of Minerals*, **30**, 293–304.

Palin, E.J., Guiton, B.S., Craig, M.S., Welch, M.D., Dove, M.T. and Redfern, S.A.T. (2003*b*) Computer simulation of Al-Mg ordering in glaucophane and a comparison with infrared spectroscopy. *European Journal of Mineralogy*, **15**, 893–901.

Palin, E.J., Dove, M.T., Sainz-Diaz, C.I. and Hernandez-Laguna, A. (2004) A computational investigation of the Al/Fe/Mg order-disorder behaviour in the dioctahedral sheet of phyllosilicates. *American Mineralogist*, **89**, 164–175.

Raudsepp, M., Turnock, A.C., Hawthorne, F.C., Sherriff, B.L. and Hartman, J.S. (1987) Characterization of synthetic pargasitic amphiboles ($NaCa_2Mg_4M^{3+}Si_6Al_2O_{22}(OH,F)_2$; $M^{3+}$ = Al, Cr, Ga, Sc, In) by infrared spectroscopy, Rietveld structure refinement and $^{27}$Al, $^{29}$Si and $^{19}$F MAS NMR spectroscopy. *American Mineralogist*, **72**, 580–593.

Redfern, S.A.T., Henderson, C.M.B., Knight, K.S. and Wood, B.J. (1997) High-temperature order disorder in $(Fe_{0.5}Mn_{0.5})_2SiO_4$ and $(Mg_{0.5}Mn_{0.5})_2SiO_4$ olivines: an *in situ* neutron diffraction study. *European Journal of Mineralogy*, **9**, 287–300.

Sainz-Diaz, C.I., Hernandez-Laguna, A. and Dove, M.T. (2001) Modelling of dioctahedral 2:1 phyllosilicates by means of transferable empirical potentials. *Physics and Chemistry of Minerals*, **28**, 130–141.

Sainz-Diaz, C.I., Palin, E.J., Hernandez-Laguna, A. and Dove, M.T. (2003*a*) Octahedral cation ordering of illite and smectite. Theoretical exchange potential determination and Monte Carlo simulations. *Physics and Chemistry of Minerals*, **30**, 382–392.

Sainz-Diaz, C.I., Palin, E.J., Dove, M.T. and Hernandez-Laguna, A. (2003*b*) Monte Carlo simulations of ordering of Al, Fe and Mg cations in the octahedral sheet of smectites and illites. *American Mineralogist*, **88**, 1033–1045.

Schröder, K.-P., Sauer, J., Leslie, M., Catlow, C.R.A. and Thomas, J.M. (1992) Bridging hydroxyl groups in zeolitic catalysts: a computer simulation of their structure, vibrational properties and acidity in protonated faujasites (H-Y zeolites). *Chemical Physics Letters*, **188**, 320–325.

Warren, M.C., Dove, M.T., Myers, E.R., Sainz-Diaz, C.I., Guiton, B.S. and Redfern, S.A.T. (2001) Monte Carlo methods for the study of cation ordering in minerals. *Mineralogical Magazine*, **65**, 221–248.

Welch, M.D. and Knight, K.S. (1999) A neutron powder diffraction study of cation ordering in high-temperature amphiboles. *European Journal of Mineralogy*, **11**, 321–331.

Welch, M.D., Kolodziejski, W. and Klinowski, J. (1994) A multinuclear NMR study of synthetic pargasite. *American Mineralogist*, **79**, 261–268.

Welch, M.D., Liu, S. and Klinowski, J. (1998) $^{29}$Si MAS NMR systematics of calcic and sodic-calcic amphiboles. *American Mineralogist*, **83**, 85–96.

Winkler, B., Dove, M.T. and Leslie, M. (1991) Static lattice energy minimization and lattice dynamics calculations on aluminosilicate minerals. *American Mineralogist*, **76**, 313–331.

[*Manuscript received 27 August 2004: revised 21 December 2004*]